

The effect of the natural degradation process on the cellulose structure of Moroccan hardwood fiber: a survey on spectroscopy and structural properties

Abdellatif Boukir^{1,*}, Ikram Mehyaoui¹, Somia Fellak¹, Laurence Asia² and Pierre Doumenq²

¹ Laboratory of Applied Chemistry, Faculty of Sciences and Techniques of Fez, Sidi Mohamed Ben Abdellah University, B.P. 2202, Imouzzar road, Fez, Morocco

² Laboratory of Environmental Chemistry, UMR CNRS 7376, MPO Team, Europôle Arbois BP 80, 13545 Aix in Provence Cedex 04; Aix-Marseille University, France

Abstract: The aim of this work is to study the effect of natural degradation on the cellulose structure conformation changes of 2 ageing Moroccan hardwoods (400 and 500 years) compared to recent one considered as a reference; and to provide information on the polymorphs content variability from two-phases material (crystalline and amorphous) influenced by a long time of ageing and environmental degradation effects. In order to investigate the effects of both natural degradation conditions and a long time of exposure on cellulose structure conformation (examined samples) with estimating their content (crystalline and amorphous cellulose), three combined techniques XRD, ATR-FTIR and FT-Raman spectroscopy were used. XRD results associated with the crystallographic planes and Miller indices provide information on the presence of a mixture of cellulose polymorphs (crystalline cellulose I, II, I_β and amorphous phase). The decrease in crystallinity-index values from recent to aged ones (38 to 19.5%) confirms well the occurred alteration of crystalline cellulose fibres and their evolution towards a high content of the amorphous form. The prominent regression in the intensities of three FTIR fingerprint cellulose regions evolving towards an overall increase in the intensities of C=O area (1733-1630 cm⁻¹) is a sign on the introduced changes on cellulose conformation and cellulose fibres degradation more accentuated in the case of the very aged sample (500 years). Similar results were confirmed by combining FT-Raman spectroscopy as a vibrational technique. No work has been done on this genus of degraded Moroccan hardwood and the relevance of this study is to investigate the compositional content and structural conformation, to determine the variability in the forms of both crystalline and amorphous cellulose phases with estimating the evolution of their polymorphism, and to monitor the degree of crystalline cellulose fibres deterioration.

Keywords: cellulose; crystallinity index and polymorphs; hardwood; X-ray diffraction (XRD); infra-red (ATR-FTIR), Raman spectroscopy.

Introduction

Cellulose component is the most abundant and renewable biopolymer in nature biosynthesized largely in the cell wall and constitute the key material for the wood, paper, textile, lumber and renewable biofuel industries¹. It is a linear polymer of D-anhydro glucopyranose units (AGU) linked by β-1,4-glycosidic bonds. Two types of AGU units exist at the end of the cellulose chain; the reducing and non-reducing end, and the cellobiose represents the repeating unit. Also, the monomer units can form either highly ordered (crystalline) or less ordered (amorphous) structures, which is due to the result of extensive interaction through intra- and intermolecular

hydrogen bonding of the three hydroxyl groups present in each cellulose macromolecules^{2,3}.

In nature, crystalline cellulose exists in four allomorphs: native cellulose I, cellulose II (prepared regeneration or alkaline treatment), cellulose III (III_I and III_{II} forms) (prepared by liquid ammonia treatment) and cellulose IV.

These cellulose allomorphs are physically different, and they differ in reactivity. New evidence suggests that cellulose IV is a slightly disordered form of cellulose I_β. Additionally, the native cellulose (crystalline fraction) presents a complex ultrastructure due to the presence of two forms for crystal phases; metastable triclinic I_α (one chain) and stable monoclinic I_β (two chain) phase⁴. Generally, the cellulose I_α is the dominant form in algae and

*Corresponding author: Abdellatif Boukir

Email address : aboukir@gmail.com

DOI : <http://dx.doi.org/10.13171/mjc8319050801ab>

Received January 22, 2019

Accepted March 23, 2019

Published May 8, 2019

bacteria, while the cellulose I_β is the dominant form in higher plants (wood and cotton) and tunicates. The main differences between the I_α and I_β structures are in crystal packing, hydrogen bonding, conformations of the anhydroglucose residues and the β -1,4 linkages⁵. As reported by Bansal et al.⁶, the crystallographic structures and hydrogen bonding arrangements for cellulose I_α and cellulose I_β provide important insights into cellulose stability and transformation and contribute toward a scientific basis for understanding cellulose bio-generation and reactivity. The relative amounts of celluloses I_α and I_β vary with the source of the cellulose, with the I_β form being dominant in higher plants⁷. It is in great importance to mention that the cellulose in its native state (cellulose I) has been reported to be more recalcitrant than its regenerated forms (cellulose II, III, etc)^{8,9}.

The cellulosic wood materials have been used for the production of novel objects in several fields due to this unique and useful property of crystallinity, because of the crystalline fraction can provide mechanical rigidity and toughness for composite materials, and constitutes a source of the recalcitrance of lignocellulosic biomass against deconstructive processes¹⁰. Whatever, the effect of serious degradation of cellulose fraction can destroy the strong intermolecular bonding, resulting in a significant change in the chemical structure of cellulose compound as well as the decrease in its crystallinity. The loss of crystallinity amount results in an enhancement in properties of flexibility, dye sorption, moisture regain, swelling and chemical reactivity, whereas density, hardness, tensile strength and dimensional stability decrease¹¹. Therefore, the determination of wood crystallinity may be an approach for understanding the effect of weathering on wood properties.

Numerous non-destructive methods as X-ray diffraction (XRD)^{10,12,13}, attenuated total reflectance-Fourier transform infrared spectroscopy (ATR-FTIR) spectroscopy^{14,15}, Raman spectroscopy¹⁰, solid-state ¹³C nuclear magnetic resonance (NMR ¹³C/CP-MAS) measurements¹⁰, and differential scanning calorimetry (DSC)¹³, were employed in several works to quantify the cellulose crystallinity and understand the structural roles of cellulose in the recalcitrant, mechanical and biological properties of plant cell walls. Lionetto et al.¹⁵, using X-ray diffraction and FTIR spectroscopy to quantify crystalline cellulose in lignocellulosic biomass, revealed that the crystallinity index (Cr.I.) of cellulose increased when wood was subjected to weathering accompanied by a considerable increase in the size of crystallites¹⁵. However, the presence of hemicellulose in lignocellulosic materials as softwoods and hardwoods reduced the crystallinity amount, whereas the syringyl lignin generated higher crystallinity¹⁶.

No work was meant to highlight the estimation of crystallinity feature and structural changes directly related to the cellulose fibers in Moroccan hardwood. Although, three non-destructive techniques incorporating ATR-FTIR, Raman and X-ray diffraction were employed in the present research to study cellulose polymer originated from argan Moroccan hardwood. Raman and Fourier transform infra-red (FTIR) spectroscopy technique for determining the crystalline absorption bands and functional groups interacting within the natural fiber and for investigating the effect of hydrogen bond on the cellulose fiber alteration. X-ray diffraction to quantify sample crystallinity based on calculated crystallinity index (Cr.I. %) and crystalline size. These methods have been applied to reveal the modification in cellulose structure occurring after the natural degradation process. A good correlation between results obtained from ATR-FTIR, Raman and XRD was found. The experimental results proved that the proposed methods might be very useful tools for accurate estimation of the degradation level of wood exposed to weathering.

Experimental

Materials

The present study was conducted on three wooden materials about different centuries originated from the Agadir region. The dimensions of wood samples are 200×200×100 mm³ (tangential × radial × longitudinal directions). The three characterized samples are listed in Table 1.

Table 1. Description of wood Samples.

Sample	Age
A _r	recent
A ₄	4 centuries
A ₅	5 centuries

X-ray diffraction measurement

The X-ray diffraction analysis was performed at room temperature with a X'Pert Pro diffractometer using CuK α monochromatic wavelength radiation at $\lambda = 1.5406 \text{ \AA}$ and generator working at 40 kV and 30 mA. The angular scanning were measured in the area of $4^\circ < 2\theta < 60^\circ$, it changes 0.016° with a step of 40s. No background correction was made.

Crystallinity index Cr.I

The crystallinity index Cr.I. % (sometimes called Segal index)¹⁷ of hardwood samples was calculated from diffraction intensity data using the following empirical equation (1)^{18,19,20,21,22}:

$$\text{Cr. I}(\%) = \left(\frac{I_{200} - I_{\text{am}}}{I_{200}} \right) \times 100 \quad (1)$$

Where I_{200} is the total intensity of diffraction of the (200) lattice peak at a $2\theta \sim 22.6^\circ$ for cellulose I ($I\beta$) and of the (020) lattice peak for cellulose II at a $2\theta \sim 21.6^\circ$, and I_{am} is the intensity of diffraction of amorphous cellulose content at a $2\theta \sim 18^\circ$ for cellulose I ($I\beta$) and at a $2\theta \sim 16^\circ$ for cellulose II (minimum intensity in this region) ¹⁸.

Crystalline size $D_{(hkl)}$

The crystalline size $D_{(hkl)}$ was calculated by the Scherrer equation (2) ²³ perpendicularly to different lattice planes $D_{(hkl)}$ from the 101, $1\bar{1}0$, 002 and 004 ^{18,20,21,22,24}.

$$D_{hkl} = K \times \lambda_1 / B_{hkl} \times \cos\theta \quad (2)$$

where $D_{(hkl)}$ is the crystalline size (nm), k is Scherrer constant: correction factor (0.89), λ_1 is X-ray wavelength (1.5406 Å), B_{hkl} is the angular full width at half maximum FWHM (sometimes called PWHM) in radians of the (hkl) line profile, and θ is the Bragg angle corresponding to the 200 plane.

Attenuated total reflectance infrared spectroscopy (ATR-FTIR)

Fourier Transform infrared (FTIR) transmission spectra were carried out through a BRUCKER VERTEX 70@ spectrometer coupled to a Hyperion@ microscope. All samples were scanned using Platinum diamond ATR (Attenuated Total Reflectance) in the wavenumber region between 4000 and 400 cm^{-1} with a resolution of 4 cm^{-1} . At each position, 16 scans were averaged. The

temperature and humidity room were controlled during analysis.

FT-Raman Spectroscopy

The FT-Raman study was conducted with a Bruker (USA) MultiRAM Stand Alone FT-Raman Spectrometer. The instrument is equipped with a diode-pumped Nd: YAG excitation source with a large emission intensity at 1.064 nm. Furthermore, the signal was collected with a liquid nitrogen cooled germanium detector. For each FT-Raman measurement, 100 scans were averaged, with a resolution of 4 cm^{-1} and time measurement of 3 min for each spectrum. All FT-Raman spectra were registered from 4000 to 250 cm^{-1} . Three analyses were performed on several locations for each sample.

Results and Discussion

X-ray

The cellulose of hardwood samples was analyzed by X-ray diffraction in order to determine both crystalline and amorphous phase as well as to estimate the amount of its crystalline fraction quantitatively. The XRD data from studied samples, over the 2θ range from 5° to 60° , have been plotted in Fig. 1. This range is more reliable to cover all of the significant intensities from both crystalline and amorphous fraction of cellulose, while the peak located in the 2θ area ranging from 34.5° to 35.2° was reserved to a mixture of the crystalline fraction (cellulose I, II, $I\beta$) ^{20,21,25}.

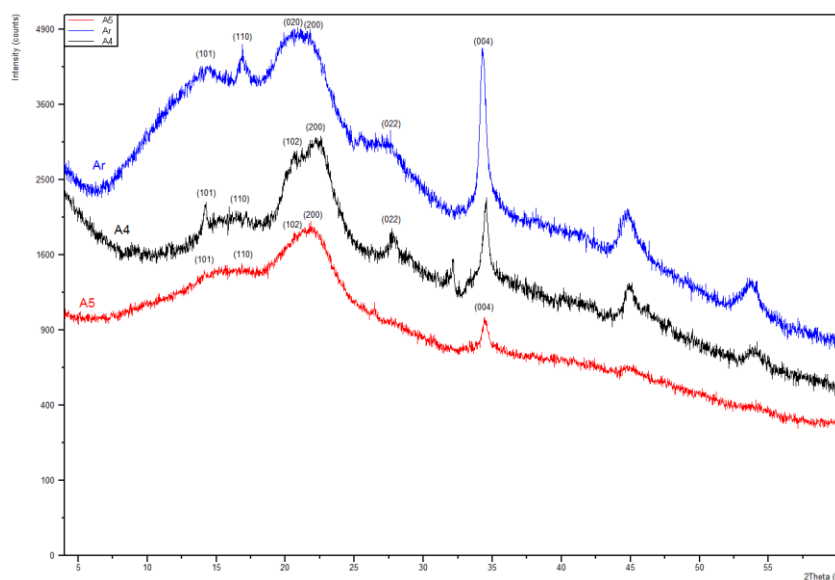


Figure 1. X-ray diffractogram of the hardwood samples

Compared to the XRD profile of cellulose from *Eucalyptus* spp. Fibres ²¹ and others woods fibres such as *Acacia* ²⁶ and *Argania Spinosa* ²⁷, the recent wood profile (Fig. 1: A_r) manifested some differences with presenting an intense broad hump between 2θ of 10° to 16° , a mixture of specific crystal sharp peak well resolved at 2θ of 16.5°

(Carrillo-Varela et al., 2018 ²¹) and an amorphous phase with a broad wide at the bottom (2θ of 16° to 18°) (Nam et al., 2016 ²⁰) closely neighboring and covering the left end of the great extent hump located between 2θ area 20° and 25° . Moreover, we can note the high increase in the intensity of the

sharp peak at 2θ of 34.5° usually known by its very low intensity and characterize the crystalline phase.

Concerning the aged samples, a significant decrease in the intensities (2θ ranging from 10° to 18° and 34.5°) was observed from A_r to A_5 , more pronounced in the case of (A_4). According to Ling et al., 2019²², in XRD feature the arising broad peaks instead of sharp ones, might be correlated to the contribution of small crystallite size which increases the breadth peak, or to the defects in the crystal lattice, and could be originated from the lacks of organization material responsible on the more diffusion in crystalline peaks.

Referring to past and recent literature data of French et Santiago Cintron 2013¹⁸, Nam et al. 2016²⁰, Ling et al. 2019²² and French 2014²⁸, all our X-ray pattern samples showed similar characteristic peaks at 2θ of 14.5° , 16.5° , 21.6° , 22.9° and 34.5° corresponding to the (101), (110) and (020), (200) and (004) crystallographic planes, respectively^{20,21,28}. The shoulder at $2\theta=20.6^\circ$ that ascribes the (102) lattice plane reflection can also be observed. According to the literature data, these diffractions correspond to the typical profile of the cellulose I allomorph^{7,21,28,29}. The trough peaks at $2\theta = 18^\circ$ between the 110 and the 200 crystallographic planes were assumed to account for the amorphous portion of cellulose²⁰.

In XRD recent sample (Fig 1: A_r), the X-ray patterns indicated the presence of peaks related to a rich fraction of both cellulose I (2θ : 14.5° , 16.5° , 22.9° and 34.5°)²¹ and cellulose II (2θ : 12° , 20° , 21.6° and 34.5°)^{20,21}. However, for the degraded sample, the decrease in the intensity of the peak at 22.9° (cellulose I) towards the formation of the new very weak peak at 2θ of 12° (A_4) and two resolved humps in the 2θ area between 20° and 23° (A_4 , A_5) which resulting in arising shoulders, is an indication on their contribution to the content of cellulose II²¹.

The consistent fraction of cellulose II was manifested by the presence of four reflections at 2θ of 12° , 20° , 21.6° attributed to the Miller indices of (1 $\bar{1}$ 0), (110) and (020) respectively, and at 2θ of 34.5° corresponding to the (004) crystallographic plane²⁸. The results obtained are in accordance with the past and more recent literature findings of French et Santiago Cintron, 2013¹⁸, Nam et al., 2016²⁰, Carrillo-Varela et al., 2018²¹, Ling et al. (2019)²² and French, 2014²⁸. Recently and with careful XRD

visual analysis, Edwards et al., 2018³⁰, assigned the peaks in the form of a shoulder at about 2θ of 12° accompanied by the peak at 2θ of 16.5° to the very small cellulose II, and the convex intensity in the 2θ area of 15° - 17° to a mixture of three celluloses: I (2θ area of 15° - 17°), II (2θ of 12° and 2θ of 16.5°) and amorphous forms (2θ area of 18°). The assignment of the weak peak at 2θ : 12° to cellulose II was supported by numerous recent literature studies^{20, 21,30}.

As presented in Fig. 1, from the recent sample (A_r) to the oldest one (A_5), all these peaks shifted to lower intensities suggesting the degradation of a crystalline form. Structural and chemical changes involved the crystalline and amorphous fraction of cellulose. Generally, amorphous cellulose is more susceptible (more reactive) than crystalline cellulose (stronger and less-reactive) to degradation process²², since it is more accessible to water, microorganisms^{14,31}. An unusual increase for the feature peak typical of (004) crystallographic plane at 34.52° was manifested in the aged sample (A_5), generally presented by a very weak intensity peak. It indicates that a partial degraded cellulose might regenerate a native crystalline form and thus, contributing to the enrichment of the relative crystalline content upon time. Another proposition is that the crystalline structure cannot be destroyed, because decreasing elasticity due to higher thermal degradation causes a lack of sheer stress which destroys the hydrogen bonding of the crystalline structure, and consequently the increase in peak intensity related to crystalline cellulose fraction³².

The changes that might occur in these fractions upon exposure to the unfavorable environment and the effect of deterioration on microcrystalline structure were also investigated based on two calculated parameters: crystallinity index and crystallite seize. The obtained values of these parameters for studied samples are plotted in Table 2. It is worth to mention that the crystallinity index of cellulose I is given by comparing the minimum in intensity above baseline at $2\theta = 16.5^\circ$ (I_{am}), and the maximum in intensity at $2\theta = 22.9^\circ$ (I_{200}), accounting for the amorphous part and the crystalline part (major diffraction from the 200 plane), respectively^{6,28,20,21,22}. This parameter varies significantly depending on the choice of the measurement method. The crystallite sizes were calculated from 101, 110 and 002 lattice planes, respectively.

Table 2. Crystallite size and Crystallinity index values of cellulose from hardwood.

Sample	D(101) (nm)	D(110) (nm)	D(020) (nm)	Cr.I (%)
A_r	-	0.56	0.408	37.96
A_4	0.622	-	0.397	25.36
A_5	0.644	-	0.419	19.50

It is shown that all amorphous cellulosic samples possessed a lower value of the crystallinity index. This can be referred to the sensibility of the analyzed sample to degradation and/or the presence of amorphous components as lignin and hemicelluloses that influence the estimation of crystallinity amount. It is reported in the literature that the presence of lignin lowers the crystallinity estimation by X-ray diffraction²⁵.

The Cr.I index value was 37.96% for the non-aged sample A_r and slightly decreased reaching 19.50% for the oldest sample A₅ (Table 2). This indicated that the crystalline region of cellulose fraction began to undergo chemical changes because of different natural degradation mechanisms as oxidation, hydrolysis. Also, the reduction of the crystalline amount of cellulose can refer to the destruction of hydrogen bonds in the crystalline cellulose fraction. The latter becomes small, and therefore, the cellulose microfibrils become harder and brittler efficiency causing efficient cut of hydrogen bonds, consequently, they become easy to destroy.

Generally, the crystalline cellulose structure is directly related to the hydrogen bonding between intermolecular hydroxyl groups and included water³³. Consequently, the loss of crystallinity is considered to result from opening of glucopyranose rings and destruction of their ordered packing³⁴. These results are by literature data, suggesting that the rapid evaporation of water causes limits the chain mobility of cellulose, and consequently, its alignment, which decreases the crystallinity feature³⁵. Thus, we can confirm that our samples underwent thermal degradation.

The small size differences may not be significant because of the calculations may have some uncertainties. So, the non-significant changes observed on D₂₀₀ crystallite size (Table 2), mean that the microcrystalline structure was not significantly affected and broken by natural degradation process. Compared to the recent sample, the crystallite sizes of both A₄ and A₅ sample showed similar values (at around 0.644) in the (101) and (020) planes, while no value was mentioned for their (110) direction planes. It means that the degradation affects a crystalline zone more than other and/or some of these zones degraded as faster than others. For the recent sample A_r, the crystallite size in (101) lattice plane could not be estimated due to the lower

intensity of these peaks and to that the crystalline regions underwent degradation at a similar extent to the amorphous regions, thus the resulting materials showed no crystallites size. A mechanism of cellulose degradation in the natural environments proceeds through a depolymerisation step, involving the amorphous regions of cellulose, until the size of oligomers becomes sufficiently small to allow metabolisation by microorganisms or solubilisation by water²⁵. Consequently, the reduction in crystallite size is correlated with the decrease in the crystalline mass fraction. It should be mentioned that the Segal crystallinity index can be influenced greatly by crystallite size³⁶.

FTIR spectroscopy

The FTIR spectra of the three analyzed samples are reported in Fig. 2 and their assignments are summarized in Table 3.

As presented in Fig. 2, the strong and broad absorption band centred at 3330 cm⁻¹ is generally characteristic of the mixture of both crystalline fractions I_β and I_α^{22,37-39} and assigned to O5-H5...O3 intramolecular hydrogen bonds in carbohydrates (cellulose crystals)^{19,37,38}. A mixture of intra- and intermolecular hydrogen bonds in cellulose are detected in the region between 3500 and 3000 cm⁻¹. Concerning the crystalline form of cellulose, the monoclinic cellulose I_β was identified by the slight peak at 3278 cm⁻¹^{22,27,39,40} related to O6-H6...O3 intermolecular hydrogen bonds in carbohydrates, while in triclinic I_α cellulose this band was detected at 3240 cm⁻¹^{22,27,40}. According to Popescu et al. 2016³⁸, the O-H intramolecular hydrogen bonds of phenolic lignin appear at 3553 cm⁻¹. Additionally, there are significant contributions from adsorbed water (weak absorption) arising from 1640 to 1620 cm⁻¹ in the amorphous region of the sample^{14,19,27,37,38,41} and at 3553 cm⁻¹ when it is weakly bonded³⁸. A noticeable decrease in the intensities of these bands with increasing time was observed in Fig. 2. It indicates effectively the water desorption phenomenon followed by the decrease in the hydrogen bond strength between the cellulosic chains, leading to the destruction of crystalline cellulose structure. Recently, Broda et Popescu 2019⁴¹ reported that the decrease in temperature reinforce the hydrogen bonds in the crystalline cellulose and microfibrils become harder and present a brittler efficiency.

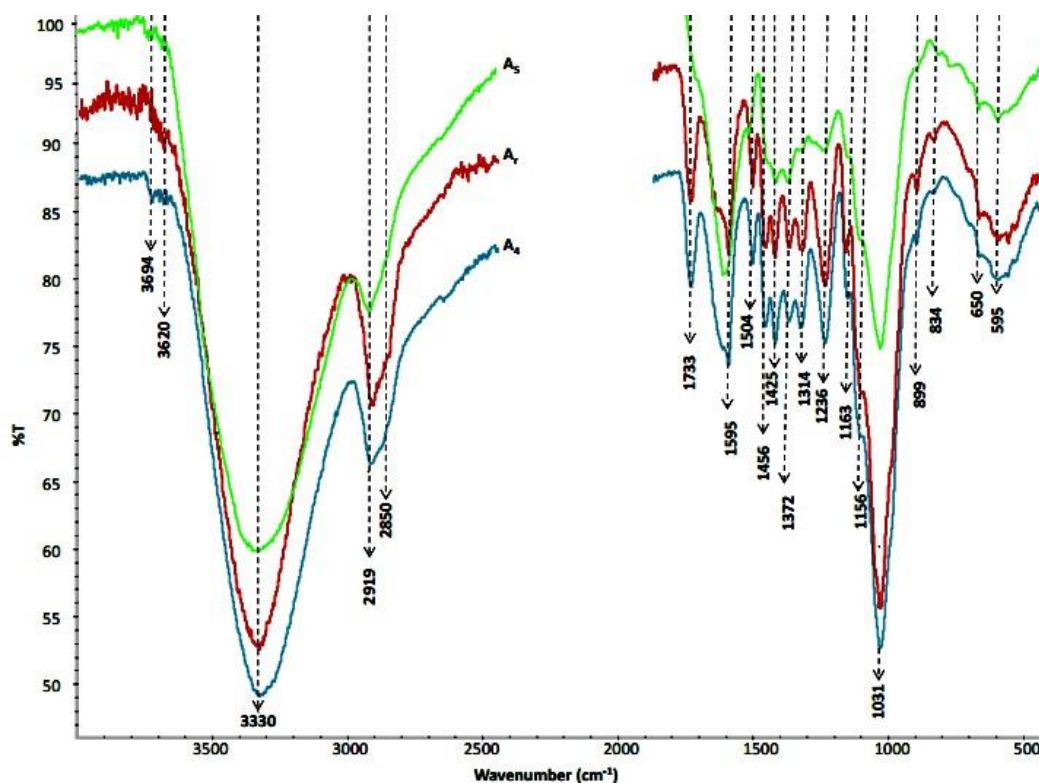


Figure 2. FTIR spectra 4000-500 cm^{-1} range acquired from hardwood samples.

Also, the cellulose of wood spectra typically shows multiple C-H (sp^3) stretching vibrations at 2850 that assigned to $\nu_s\text{CH}_2$ and 2919 cm^{-1} ascribed to $\nu_{as}\text{CH}_2$ and $\nu\text{C-H}$ in cellulose, and to $\nu_s\text{CH}_3$ (methoxyl group) in lignin^{19,22,37,38}. Recently, Ling et al. 2019²² attributed the signal at 2944 cm^{-1} to cellulose I_β accompanied with a shoulder at 2968 cm^{-1} . As shown in Fig. 2, each FTIR spectrum presents the main characteristic peaks related to the mixture of crystallized and amorphous cellulose fractions. The presence of crystalline cellulose is confirmed by the three following signals at 1456 cm^{-1} ^{27,37,39,42}, 1372 cm^{-1} ^{19,22,42,44} and 1314 cm^{-1} ^{19,22,27,37-41,44} (bending mode vibration of C-H), while the amorphous content is justified by the presence of centered peak at 1425 cm^{-1} corresponding to δCH_2 bending vibration (*scissoring*)^{16,19,27,39,40,43}. According to Song et al. 2015⁴² and Zghari et al. 2018³⁷ the crystalline cellulose I and cellulose II appear as doublet peak at 1430 cm^{-1} (strong band) and at 1420 cm^{-1} (weak band), respectively⁴⁴. Furthermore, Hajji et al. 2015¹⁹ and Broda et al. 2019⁴¹ report that the decline in the intensities of the two bands at 1314 and 1163 cm^{-1} is correlated to the decrease of cellulose crystallinity (cellulose I). Usually in amorphous cellulose (disordered structure), these bands were located at 1336 and 1156 cm^{-1} , respectively.

The two absorptions bands at 1163 and 1156 cm^{-1} are related to the crystalline and amorphous form of cellulose, respectively, characteristics of the C-O-C asymmetric bridge stretching vibration of the glycosidic ring. According to a recent study by Ling

et al. 2019²², the introduced transformation of the two bands is considered as a key of included changes on fingerprint cellulose area, informing well on both distortions of crystalline arrangements and smaller crystallinity index. Similar spectral changes have been observed in our case study from recent sample A_r to aged ones (A_4 and A_5) indicating the conversion of crystalline content towards an amorphous fraction. This finding supports the hypothesis of distortion in cellulose crystalline arrangements. The fingerprint region of cellulose with prominent signal centred at 1031 cm^{-1} (C-O) is gradually shifted to the lower intensity from recent to altered sample A_5 . Additionally, the visible and notable reduction indicate well the occurred changes in the structural conformation of the aged cellulose sample (A_5) which is more affected after 500 years of exposure to natural environmental degradation process.

Concerning the band at 899 cm^{-1} ascribed to C-O-C stretching vibration mode of cellulose β -(1-4)-glycosidic linkage is related to the content of amorphous cellulose which is completely in accordance with published literature studies^{16,19,22,38,39,43}. However, this band is sensitive to changes, and so, a portion of amorphous cellulose content underwent crystallization due to mechanochemical processes²² and/or to natural environmental degradation conditions^{37,42,44}; that is why it is subject of many controversies data^{22,37,42,44}. A clear indications have been reported by Song et al. 2015⁴² which attributed the *weak* and *broad* absorption band to cellulose I, while the *strong* and

sharp one might be assigned to cellulose II and amorphous cellulose. The similar finding was confirmed by Hajji et al. 2016⁴⁴ and Zghari et al. 2018³⁷ which reported that the ageing process promote the breakage of the C-O-C bonds of crystalline cellulose I in the β -(1-4)-glycosidic linkage.

In recent literature data, Ling et al. 2019²² correlated the weak signal at 720 cm^{-1} to the presence of a small amount of cellulose I_{β} and

ascribed it to CH_2 rocking vibration^{37,40}, while the tiny peak at 750 cm^{-1} attributed to a small amount of cellulose I_{α} , the latter is supported by the presence of O-H stretching vibration mode at 3240 cm^{-1} ^{22,40}.

The FTIR crystalline and amorphous results correlate well with the crystallinity index values measured in XRD section (X-ray diffraction, Table 2).

Table 3. Assignments of the main vibrations of cellulose in the hardwood FTIR spectra.

Wavenumber (cm^{-1})	Assignment	Cellulose fraction	Reference
3330	$\nu(\text{OH})$ stretching vibration of alcohol-bonded hydroxyl groups	crystalline I_{β} + I_{α}	22,38,39,37
3278	O6 H6...O3 intermolecular hydrogen bonds	cellulose I_{β}	22,27,39,40
3000-2850	$\nu_{as}\text{CH}_2$ and $\nu_s\text{CH}_2$ in methylene and $\nu_{as}\text{CH}_3$, $\nu_s\text{CH}_3$ in methyl groups	crystalline and amorphous	39,40,44
2900	$\nu\text{C-H}$ stretching vibration	crystalline	22, 39,43
1456	δCH_2 asymmetric bending mode (scissoring)	crystalline	27,37,39,42
1425	δCH_2 symmetric bending (scissoring) crystalline cellulose I at 1430 cm^{-1} (strong) ^{39,43} and crystalline cellulose II at 1420 cm^{-1} (weak) ^{37,42} O-C-H in plane bending vibration ^{37,42}	amorphous	42,43,19,37, 39,40,27, 16
1372	$\delta\text{C-H}$ bending vibration	crystalline	22,42,43,44, 19, 37,39,27
1314	δCH_2 rocking ⁴⁰	crystalline	22,27,19,37, 40,38,39,44
1163	C-O-C asymmetric bridge stretching vibration	crystalline	22,37,38,40, 27,43
1156		moreover, amorphous	
1110	C-O-H anti-asymmetric in-plane stretching vibrations	crystalline and amorphous	22,37,39,43
899	$\nu\text{C}_1\text{-O-C}$ of β -(1-4)-glycosidic linkage bond (weak and broad in cellulose I, but strong and sharp in cellulose II and amorphous cellulose) ^{37,42} and references cited	amorphous + (a portion of this band is sensitive to change and might undergo crystallization)	16,19,22,27, 37,38,43 37,39,42,44
720	CH_2 rocking vibration in cellulose I_{β} (cellulose I_{α} appear generally as a tiny peak at 750 cm^{-1} and 3240 cm^{-1} ^{22,37,40})	a small amount of cellulose I_{β}	22,27,37,40
650	$\delta\text{O-H}_{oop}$ out of plane bending mode (weak and broad band)	cellulose crystalline	37,40

The feature of crystallinity was influenced by different types of degradation mechanism, such as oxidation and hydrolysis. It increases the intensity of the C=O band, especially in the sample dating from the 15th centuries (Fig. 2 A₅). This could be justified by the presence of a large and intense absorption band between 1650-1732 cm^{-1} ascribed to the

stretching vibration of the C=O group, informing on the pronounced alteration^{19,37,38,44}. As can be illustrated in Fig 3, the opening chain which is the result of oxidation mechanism occurred on cellulose can be undergoing to the other types of oxidation resulting in another type of compound.

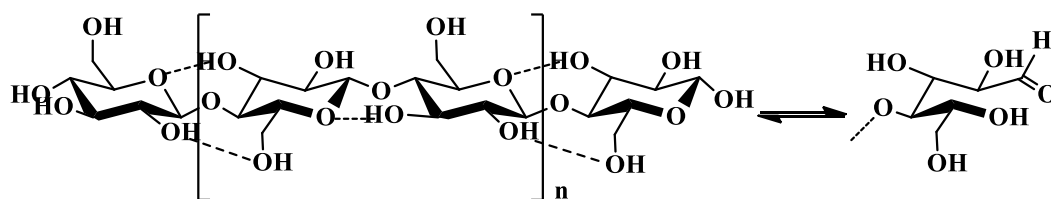


Figure 3. Structure of cellulose $(C_6H_{10}O_5)_n$ polymer adapted from Fengel and Wegener⁴⁵ (the repeating cellobiose unit is evidenced within the square brackets).

According to Agarwal et al.¹⁶, the presence of lignin and hemicelluloses influences the amount of the crystalline form of cellulose fibers, and the lignin fraction is the most responsible for this evolution. The presence of the later fraction in all spectra (Fig. 2) is manifested by the following absorptions bands at 1595 and 1504 cm^{-1} assigned to the $\nu C=C_{ar}$ skeletal vibration in the phenolic ring (lignin motif type guaiacyl, ie coniferyl) and at 1236 cm^{-1} attributed to $\nu C_{ar}-O$ in lignin^{27,37,38}. Generally, a weak 1595 cm^{-1} band stands for non-polar aromatic compounds, while a strong one stands for polar aromatic compounds such as phenols^{27,38,46}. In our case study, the very strong 1595 cm^{-1} absorption indicates well the presence of high polar aromatic compounds of lignin (aromatic ring substituted by hydroxyl and/or methoxy groups : guaiacyl, ie conifer). The obtained result showed an excellent correlation with FT-Raman data (next section).

The small sharp detected at 897 cm^{-1} (Fig. 2) represents the glycosidic C_1-H deformation with ring vibration contribution, which is characteristic of $\beta(1-4)$ glycosidic linkages between glucose in amorphous cellulose^{14,16,19,27,37,40}. According to S. Acharya et al.³⁹, the ratio of integrated peaks at 1427 and 899 cm^{-1} (A_{1427}/A_{899}) has been used in order to estimate the IR empirical crystallinity index of cellulose, while in recent study conducted by²² various IR peak ratios have been proposed using the three following ratios (A_{1372}/A_{895} , A_{1430}/A_{894} , A_{1372}/A_{2900}). It should be noted that the amorphous area of the cellulosic component was less affected by the degradation process. According to Boukir et al.⁴⁶ and Zghari et al.³⁷, the broad signal at 650 was attributed to OH out of plane bending^{10,27,39,40}.

FT-Raman spectroscopy

The FT-Raman technique was used to obtain more structural information on the hardwood cellulose samples. The FT-Raman spectra of the three samples are illustrated in Fig. 4. The complexity of FT-Raman spectra is due to the presence of many signals related to the cellulose, hemicelluloses and lignin which create a polymeric matter that produce a complex wooden matrix. All

FT-Raman bands assignment related to the analysed materials were summarized in Table 4.

The FT-Raman spectra of cellulosic fibers can be visually divided into three regions (Fig. 4): 3350-2700 cm^{-1} , 1750-800 cm^{-1} and 610-150 cm^{-1} that include, respectively, methyl and methylene stretching vibrations, methyl bending and rocking as well as C-O-H in-plane bending and the skeletal bending vibrations (e.g. C-C-C, C-O-C, O-C-C and O-C-O)^{47,48}.

The broad CH stretching vibration band at 2897 cm^{-1} characterize the CH_2 group in the glucopyranose ring of cellulose I_{β} ¹⁰. The doublet band at 1094 cm^{-1} and 1119 cm^{-1} were assigned to the symmetric and asymmetric $\beta(1,4)$ -glycosidic linkage stretching modes, respectively^{47,49}. The intensity ratio between these later provides information on the hydrolytic cleavage of the glycosidic ether bonds of the cellulosic chains. According to Kavkler and Demsar⁵⁰, this ratio can be used as an indicator of ageing in different historic specimens. While, the disappearance of these two bands is a sign on an advance cellulose degradation step⁵¹. In recent literature studies, Ling et al. 2019²², Makarem et al. 2019⁵² and Agarwal et al. 2016⁵³ reported that the regression of the two main bands at 1096 cm^{-1} (fingerprint cellulose: broad and very intense) and 2900 cm^{-1} is an indication on the distortion of crystalline arrangements, and thus, resulting a reduction of Cr.I.. The same trends have been shown in our samples from recent (A_r) to aged one (A_4) but more pronounced until the disappearance of all the bands in the case of very aged one (A_5), confirming well the complete deterioration of cellulose (Fig. 4). Additionally, the amorphous cellulose fraction is detected in the Raman spectra by the presence of the following signals at 1455 cm^{-1} ^{22,47} assigned to H-C-H bending with the contribution of smaa II proportion of H-OC bending, and at 896 cm^{-1} ascribed to the C-H deformation⁴⁷. The two latter signals (amorphous content) influenced by the degradation phenomena underwent the same fate such others absorption bands (1096, 2900 cm^{-1}).

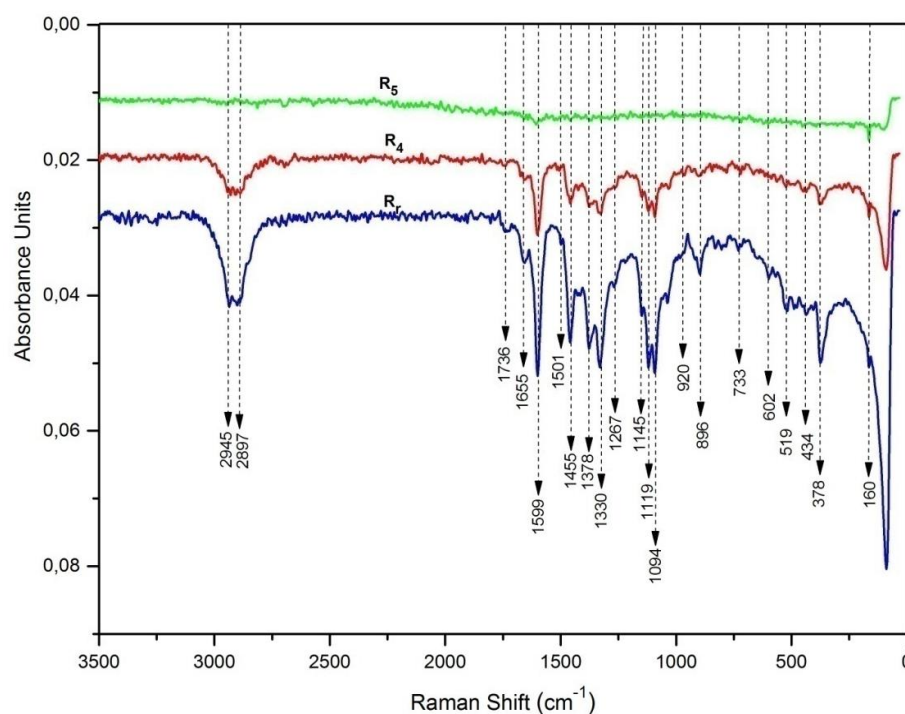


Figure 4. FT-Raman spectra 3500-0 cm^{-1} range acquired from hardwood samples.

The detected absorptions between 1300 and 1410 cm^{-1} were characteristic of δCH_2 modes. Generally, the bands at 1476, 1455 and 431 cm^{-1} (bending δCCO and δCCC) are typical for crystalline cellulose I⁵⁰. The arising peak at 519 cm^{-1} informs on the presence of glycosidic linkage deformation in hemicelluloses (δCOC , δCCC). The decrease in the intensities of these bands ascribed to loss of the structural order when interchain hydrogen

bonds are broken, followed by the cleavage of glycosidic linkages that shortened chains, leading to the decrease of crystallinity depending on the prolonged sample age. The results obtained by FT-Raman seem to be in complete agreement with the crystallinity index values measured in XRD section (X-ray diffraction, Table 2) and match well with those of FTIR data (FTIR spectroscopy section).

Table 4. Main bands vibrations in hardwood cellulose samples FT-Raman spectra.

Wavenumber (cm^{-1})	Assignments	Fraction	References
2897	νCH and νCH_2	cellulose I β	22,47,52,53
1455-1462	HCH bending and small proportion of HOC bending	amorphous cellulose	22,47,51,54
1378	CH_2 wagging mode		47,55
1331 + 1119 + 990 +	bending vibrations of cellulose glycosidic linkages and/or Coupled C-O-C and CC stretching modes	amorphous cellulose	22,10,47,51,55,
1094	Coupled C-O-C and CC stretching modes	crystalline cellulose	22,52,53,47,10,51,55
896	CH deformation	amorphous cellulose	47,51
763	β -anomer glucopyranose (very weak band)		
519	CCO deformations of β -anomer glucopyranose	cellulose	55
431	$\delta(\text{CCO})$	crystalline cellulose	54
378	symmetric bending vibration of pyranose rings and/or $\delta_s(\text{CCC})$	crystalline cellulose	22,52,53,47,51,54

It is noteworthy that the evolution of cellulose crystallinity was influenced by the presence of amorphous content, such as lignin and

hemicelluloses. In our spectra, this can be confirmed by the typical bands at 1655, 1599 and 1267 cm^{-1} that correspond, respectively, to the conjugated C=C

stretching vibration of coniferyl alcohol (guaiacyl) overlapping with $\nu\text{C=O}$ group of coniferyl acid after alcohol oxidation in side chain, and with polar aromatic C=C in phenolic compounds related to guaiacyl and syringyl monomers in lignin^{10,47}.

The region bands between 300 and 600 cm^{-1} cannot be unambiguously attributed to certain vibrations, and might be assigned to $\delta\text{C-C-C}$ deformation in crystalline fraction of cellulose^{22,47,50,52-55}, while Dudek et al.⁵⁵ have considered this region as a key of the information and signature of the absolute configuration of the anomeric centre of glycosidic sugar.

Conclusion

The present work developed a detailed evaluation of cellulose structure as a component of Moroccan hardwood materials as well as the changes that occur at its microcrystalline fraction. Based on the X-ray diffraction obtained results, the cellulose lost its property of crystallinity during exposure time to the natural degradation process. The FTIR spectroscopy and FT-Raman results converge towards the conclusion that the evolution of cellulose crystallinity was influenced by the presence of lignin and hemicelluloses. The used methods were considered as ones of the best vibrational techniques that can be applicable to analyze cellulose polymorphs and evaluate, exhaustively, crystallinity behaviors as well as structural changes on other wood components as lignin and hemicelluloses.

Acknowledgement

The authors would like to thank Professor P. Doumenq and Dr L. Asia (Aix-Marseille University, Laboratory of Environment Chemistry, Aix en Provence Cedex 4, France) for recording the FT-IR spectra.

References

- 1- Y. B. Park, K. Kafle, C. M. Lee, D. J. Cosgrove, S. H. Kim, Does cellulose II exist in native alga cell walls? Cellulose structure of *Derbesia* cell walls studied with SFG, IR and XRD, *Cellulose*, **2015**, 22, 3531-3540.
- 2- P. K. Gupta, V. Uniyal, S. Naithani, Polymorphic transformation of cellulose I to cellulose II by alkali pretreatment and urea as an additive, *Carbohydr. Polym.*, **2013**, 94, 843-849.
- 3- L. Donaldson, B. Nanayakkara, J. Harrington, *Wood Growth and Development*; Elsevier, *Encyclopedia of Applied Plant Sciences* (Second Edition), **2017**, 1, pp. 203-210.
- 4- Y. Kataoka and T. Kondo, FT-IR Microscopic Analysis of Changing Cellulose Crystalline Structure during Wood Cell Wall Formation, *Macromolecules*, **1998**, 31, 760-764.
- 5- H. Kono, S. Yunoki, T. Shikano, M. Fujiwara, T. Erata, M.J. Kawai, CP/MAS ^{13}C NMR Study of Cellulose and Cellulose Derivatives. 1. Complete Assignment of the CP/MAS ^{13}C NMR Spectrum of the Native Cellulose, *J. Am. Chem. Soc.*, **2002**, 124, 7506-7511.
- 6- P. Bansal, M. Hall, M.J. Realff, J.H. Lee, A.S. Bommarius, Multivariate statistical analysis of X-ray data from cellulose: a new method to determine degree of crystallinity and predict hydrolysis rates, *Bioresour. Technol.* **2010**, 101, 4461-4471.
- 7- S. Park, J. O. Baker, M. E. Himmel, P. A. Parilla, D. K. Johnson, Cellulose crystallinity index: Measurement techniques and their impact on interpreting cellulase performance, *Biotechnol. Biofuels*, **2010**, 3, 1-10.
- 8- S.P.S. Chundawat, G. Bellesia, N. U. ppugundla, L. da Costa Sousa, D. Gao, A. M. Cheh, U. P. Agarwal, C. M. Bianchetti, G. N. Phillips, P. Langan, V. Balan, S. Gnanakaran, B. E. Dale, Restructuring the crystalline cellulose hydrogen bond network enhances its depolymerization rate, *J. Am. Chem. Soc.*, **2011**, 133, 11163- 11174.
- 9- J. Zhang, Y. Wang, L. Zhang, R. Zhang, G. Liu, G. Cheng, Understanding changes in cellulose crystalline structure of lignocellulosic biomass during ionic liquid pretreatment by XRD, *Bioresour. Technol.*, **2014**, 1 51, 402-405.
- 10- A.L. Barnette, C. Lee, L.C. Bradley, E.P. Schreiner, Y.B. Park, H. Shin, D.J. Cosgrove, S. Park, S.H. Kim, Quantification of crystalline cellulose in lignocellulosic biomass using sum frequency generation (SFG) vibration spectroscopy and comparison with other analytical methods, *Carbohydr. Polym.* **2012**, 89, 802-809.
- 11- Z.H. Jiang, Z. Yang, C. L. So, C. Y. Hse, Rapid prediction of wood crystallinity in *Pinus elliotii* plantation wood by near-infrared spectroscopy, *J. Wood. Sci.*, **2007**, 53, 449-453.
- 12- K. Labidi, O. Korhonen, M. Zrida, A. H. Hamzaoui, T. Budtova, All-cellulose composites from alfa and wood fibers, *Ind. Crops. Prod.*, **2019**, 127, 135-141.
- 13- D. Ciolacu, F. Ciolacu, V. I. Popa, Amorphous cellulose- structure and characterization, *Cell. Chem. Technol.*, **2011**, 45, 13-21.
- 14- D. Tamburini, J. J. Łucejko, M. Zborowska, F. Modugno, E. Cantisani, M. Mamonov, M. P. Colombini, The short-term degradation of cellulosic pulp in lake water and peat soil: A multi-analytical study from the micro to the molecular level, *Int. Biodeterior. Biodegradation*, **2017**, 116, 243-259.
- 15- F. Lionetto, R. D. Sole, D. Cannoletta, G. Vasapollo, A. Maffezzoli, Monitoring Wood Degradation during Weathering by cellulose crystallinity, *Materials*, **2012**, 5, 1910-1922.

- 16- U. P. Agarwal, S. A. Ralph, R. S. Reiner, C. Baez, new cellulose crystallinity estimation method that differentiates between organized and crystalline phases, *Carbohydr. Polym.*, **2018**, 190, 262-270.
- 17- L. Segal, J.J. Creely, A.E. Martin, C.M. Conrad, An empirical method for estimating the degree of crystallinity of native cellulose using the X-ray diffractometer. *Text. Res. J.*, **1959**, 29, 786-794.
- 18- A. D. French, M. Santiago Cintrón; Cellulose polymorphy, crystallite size, and the segal crystallinity index, *Cellulose*, **2013**, 20, 583-588.
- 19- L. Hajji, A. Boukir, J. Assouik, A. Kerbal, M. Kadjout, P. Doumenq, M. L. De Carvalho, A Multi-analytical Approach for the Evaluation of the Efficiency of the Conservation-Restoration Treatment of Moroccan Historical Manuscripts dating to 16th, 17th and 18th centuries, *Appl. Spectrosc.*, **2015**, 69, 920-938.
- 20- S. Nam, A. D. French, B. D. Condon, M. Concha; Segal crystallinity index revisited by the stimulation of X-ray diffraction patterns for cellulose I β and cellulose II. *Carbohydr. Polym.*, **2016**, 135, 1-9.
- 21- I. Carrillo-Varela, M. Pereira, R. T. Mendonça; Determination of polymorphic changes in cellulose from *Eucalyptus* spp. Fibres after alkalization. *Cellulose*, **2018**, 25, 6831-6845.
- 22- Z. Ling, T. Wang, M. Makarem, M. Santiago Cintrón; S. Nam, J. V. Edwards, S. H. Kim, F. Xu, A. D. French; Effects of ball milling on the structure of cotton cellulose. *Cellulose*, **2019**, 26, 305-328.
- 23- P. Scherrer, Bestimmung der Größe und der inneren Struktur von kolloidteilchen mittels röntgenstrahlen. *Nachrichten von der Gesellschaft der Wissenschaften zu Göttingen*, **1918**, 26, 98-100.
- 24- H.L. Chen, A. Yokochi, X-Ray Diffractometric Study of Microcrystallite Size of Naturally Colored Cotton *J. Appl. Polym. Sci.*, **2000**, 76, 1469.
- 25- X. Ju, M. Bowden, E. E. Brown, X. Zhang, An improved X-ray diffraction method for cellulose crystallinity measurement, *Carbohydr. Polym.*, **2015**, 123, 476-48.
- 26- M. Danish, R. Hashim, M.N. Mohamad Ibrahim, M. Rafatullah, O. Sulaiman, Surface characterization and comparative adsorption properties of Cr(VI) on pyrolysed adsorbents of *Acacia mangium* wood and *Phoenix dactylifera* L. stone carbon. *J. Anal. Appl. Pyrol.*, **2012**, 97, 19-28.
- 27- A. Boukir, S. Fellak, P. Doumenq, Structural Characterization of *Argania Spinosa* Moroccan Wooden Artifacts during natural degradation progress using Infrared Spectroscopy (ATR-FTIR), X-Ray Diffraction (XRD) and Scanning Electron Microscopy (SEM), *Heliyon*, **2019** (*under revision*).
- 28- A. D. French; Idealized powder diffraction patterns for cellulose polymorphs. *Cellulose*, **2014**, 21, 885-896.
- 29- E. L. Hult, T. Iversen, J. Sugiyama, Characterization of the supermolecular structure of cellulose in wood pulp fibres. *Cellulose*, **2003**, 10, 103-110.
- 30- J.V. Edwards, K. Fontenot, F. Liebner, N. Doyle nee Pircher, A. D. French, B.D. Condon.; Structure/Function Analysis of Cotton-Based Peptide-Cellulose Conjugates: Spatiotemporal/Kinetic Assessment of Protease Aerogels Compared to Nanocrystalline and Paper Cellulose. *Int. J. Mol. Sci.* **2018**; 19, 840.
- 31- R. M. Rowell, R. Pettersen, J. S. Han, J. S. Rowell, M.A., Tshabalala, Cell wall chemistry. In: Rowell, R.M. (Ed.), *Handbook of Wood Chemistry and Wood Composites*. CRC, Boca Raton, London, New York, Singapore, **2005**, pp. 37-76.
- 32- R. Shimura, A. Nishioka, I. Kano, T. Koda, T. Nishio, Novel method for producing amorphous cellulose only by milling, *Carbohydr. Polym.*, **2014**, 102, 645-648.
- 33- C. M. Popescu, M. C. Popescu, C. Vasile, Structural changes in biodegraded lime wood, *Carbohydr. Polym.*, **2010**, 79, 362-372.
- 34- U. J. Kim, S. Kuga, M. Wada, T. Okano, T. Kondo, Periodate oxidation of crystalline cellulose, *Biomacromolecules*, **2000**, 1, 488-492.
- 35- J. Rojas, V. Kumar, Effect of polymorphic form on the functional properties of cellulose: A comparative study, *Carbohydr. Polym.*, **2012**, 87, 2223-2230.
- 36- M. C. I. Mohd Amin, A. G. Abadi, H. Katas, Purification, characterization and comparative studies of spray-dried bacterial cellulose microparticles, *Carbohydr. Polym.*, **2014**, 99, 180-189.
- 37- B. Zghari, L. Hajji, A. Boukir, Effect of Moist and Dry Heat Weathering Conditions on Cellulose Degradation of Historical Manuscripts exposed to Accelerated Ageing: ¹³C NMR and FTIR Spectroscopy as a non-Invasive Monitoring Approach. *J. Mater. Environ. Sci.*, **2018**, 9, 641-654.
- 38- C. M. Popescu, P. Gradinariu, M. C. Popescu, by white rot fungi through infrared and two-dimensional correlation spectroscopy, *J. Mol. Struct.*, **2016**, 1124, 78-84.
- 39- S. Acharya, Y. Hu, H. Moussa, N. Abidi, Preparation and characterization of transparent cellulose films using an improved cellulose dissolution process. *J. Appl. Polym. Sci.*, **2017**, 134, 44871. DOI: 10.1002/APP.44871.
- 40- M. Schwanninger, J. C. Rodrigues, H. Pereira, B. Hinterstoisser, Effects of short-time vibratory ball milling on the shape of FT-IR

- spectra of wood and cellulose, *Vib. Spectrosc.*, **2004**, 36, 23-40.
- 41- M. Broda, C. M. Popescu, The natural decay of archaeological oak wood versus artificial degradation processes: an FT-IR spectroscopy and X-ray diffraction study, *Spectrochim. Acta Part A: Mol. Biomol. Spectro.*, **2019**, 136, 1038-1046.
- 42- Y. Song, J. Zhang, X. Zhang, T. Tan, The correlation between cellulose allomorphs (I and II) and conversion after removal of hemicellulose and lignin of lignocellulose. *Bioresour. Technol.*, **2015**, 193, 164-170.
- 43- N. Abidi, L. Cabrales, C.H. Haigler, Changes in the cell wall and cellulose content of developing cotton fibers investigated by FTIR spectroscopy. *Carbohydr. Polym.*, **2014**, 100, 9-16.
- 44- L. Hajji, A. Boukir, J. Assouik, S. Pessanha, M. L. De Carvalho, Artificial ageing paper to assess long term effects of conservative treatment. Monitoring by Infrared spectroscopy (ATR-FTIR), X-ray diffraction (XRD) and Energy dispersive X-ray fluorescence (EDXRF), *Microchem. J.*, **2016**, 124, 646-656.
- 45- D. Fengel and G. Wegener, *Wood, Chemistry, Ultrastructure, Reactions*. Waster & Grugter, New York, **1984**, pp: 613.
- 46- A. Boukir, M. Guiliano, L. Asia, G. Mille, A fraction to fraction study of photooxidation of BAL 150 crude oil asphaltene, *Analisis*, **1998**, 26, 358-364.
- 47- S. Fellak, A. Boukir, Moroccan Cedar softwood study: Application of FT-Raman spectroscopy, *MATEC Web. Conf.*, **2018**, 191, 00014. <https://doi.org/10.1051/mateconf/201819100014>.
- 48- Y. Essaadaoui, A. Lebkiri, EL H. Rifi, L. Kadiri, A. Ouass, Adsorption of cobalt from aqueous solutions onto Bark of Eucalyptus. *Mediterr. J. Chem.*, **2018**, 7, 145-155.
- 49- K. Schenzel, S. Fischer, NIR FT Raman Spectroscopy: A rapid analytical tool for detecting the transformation of cellulose polymorphs, *Cellulose*, **2001**, 8, 49-57.
- 50- K. Kavkler, A. Demsar, Examination of cellulose textile fibres in historical objects by micro-Raman spectroscopy, *Spectrochim. Acta Part A: Mol. Biomol. Spectro.*, **2011**, 78, 740-746.
- 51- M. Petrou, H.G. M. Edwards, R.C. Janaway, G.B. Thompson, A.S. Wilson, Fourier-transform Raman spectroscopic study of a Neolithic waterlogged wood assemblage, *Anal. Bioanal. Chem.*, **2009**, 395, 2131-2138.
- 52- M. Makarem, CM, Lee, K. Kafle, S. Huang, I. Chae, H. Yang, J.D. Kubicki, S.H. Kim, Probing cellulose structures with vibrational spectroscopy, *Cellulose*, **2019**, 26, 35-79.
- 53- U. P. Agarwal, S. A. Ralph, R. S. Reiner, C. Baez, Probing crystallinity of never-dried wood cellulose with Raman spectroscopy, *Cellulose*, **2016**, 23, 125-144.
- 54- N. Gierlinger, S. Luss, C. Konig, J. Konnerth, M. Eder, P. Fratzl, Cellulose microfibril orientation of *Picea abies* and its variability at the micron-level determined by Raman imaging, *J. Exp. Bot.*, **2010**, 61, 587-595.
- 55- M. Dudek, G. Zajac, E. Szafraniec, E. Wiercigroch, S. Tott, K. Malek, A. Kaczor, M. Baranska, Raman Optical Activity and Raman spectroscopy of carbohydrates in solution, *Spectrochim. Acta Part A: Mol. Biomol. Spectro.*, **2019**, 206, 597-612.